A WAVELET TRANSFORM APPLIED TO ACOUSTIC EMISSION SIGNALS: PART 2: SOURCE LOCATION[#]

M. A. HAMSTAD[+], A. O'GALLAGHER and J. GARY

National Institute of Standards and Technology, Materials Reliability Division (853),
Boulder, CO 80305-3328;
[+]Also Department of Engineering, University of Denver, Denver, CO 80208.

Abstract

In Part 2, the same finite-element-generated database of acoustic emission (AE) signals was used, as in Part 1: Source Identification, to examine the application of a wavelet transform (WT) to improve the accuracy of AE source location. These signals represented the top surface out-of-plane displacement versus time from buried dipole sources in aluminum plates 4.7 mm thick. The method utilizes a WT result to select AE signal-arrival times for a single group velocity from energetic modes. The cases of both the large plate without edge reflections and the small plate (coupon) with multiple edge reflections were examined. The arrival time of a specific frequency of an energetic fundamental mode of the far-field signals was determined from the WT. Using these arrival times at three propagation distances, a group velocity was determined for comparison with the appropriate group velocity based on dispersion curves. Both filtered narrow-band (100 to 300 kHz) and wideband (40 kHz high-pass) signals were examined. In addition, in the large-plate case, experimental sensor/preamplifier electronic noise was added to the AE signals to examine the effect of noise on the determination of accurate arrival times as a function of signal-to-noise (S/N) ratios. Results for the large plate indicate that very accurate arrival times can be determined that correspond to a particular group velocity. In the coupon case, the results indicate significant distortions in the arrival times due to the multiple edge reflections. The perturbation due to the presence of electronic noise was relatively small for the case of the wideband signals in the large plate until signal-to-noise ratios reached levels where an AE hit would likely not be recorded.

1. Introduction

One of the important aspects of acoustic emission (AE) technology is the ability to use the arrival times of the signals (from a single event) at three or more sensors to calculate the location of the source in the test object. Often the two-dimensional location in a plate is determined. The standard technique combines the measured arrival times with an appropriate single propagation velocity to calculate the source location. In most AE applications, the arrival times of the signals are obtained from the time that the signals first penetrate a fixed voltage threshold. As has been documented (Hamstad, 1986; Gorman, 1990; Hamstad and Downs, 1995), this approach leads to location errors. In particular, the arrival times at the different sensors often are determined from different unknown velocities. This situation is a direct result of both the AE source characteristics (for example the source strength) and effects of the propagation of dispersive Lamb waves along with geometry-based attenuation. The net result is that source location may be calculated on the basis of inconsistent data. Specifically, the arrival times are not all obtained at the same

[#] Contribution of the U.S. National Institute of Standards and Technology; not subject to copyright in the US.

velocity, and the velocity used in the location calculation is not the correct one for each sensor hit.

Some previous research has demonstrated an approach to decrease the location errors (Ziola and Gorman, 1992). In this approach, cross-correlation techniques were used to determine the arrival times for a particular mode (typically the flexural mode) and frequency. The AE signals analyzed were obtained from sensors responding to out-of-plane surface displacements. These arrival times were combined with a corresponding theoretical group velocity to calculate a more accurate source location. The resulting improvement in location accuracy was demonstrated by out-of-plane pencil-lead breaks on the surface of a plate test specimen. This validation approach is potentially incomplete. First, out-of-plane lead breaks create relatively large flexural mode (anti-symmetric) components of the AE signals as compared to real AE sources, which can be dominated by in-plane dipoles with smaller flexural-mode signals. Second, the surface lead breaks do not account for the substantial differences in the dominate mode in AE signals as a function of the depth of a real AE source through the plate thickness, as was shown in Part 1 (Hamstad et al., 2002).

In the research reported here, we examine the use of a wavelet transform (WT) to accurately obtain arrival times at known group velocities from realistic modeled AE signals. We utilized AGU-Vallen Wavelet program for obtaining WTs as in Part 1 (Hamstad et al., 2002). The AGU group first used WT for determining the group velocity dispersion of the Lamb waves (Cho et al., 1996; Hayashi et al., 1999) and for AE source location on anisotropic CFRP plates (Yamada et al., 2000; Takemoto et al., 2000). Yamada et al. (2000) determined the group velocity of flexual Lamb waves (generated by pencil-lead breaks or ball drops) from the maxima of WT coefficients of a certain frequency. A few other research works used a WT for AE source location (Yamada et al., 2000; Takemoto et al., 2000; Kwon and Joo, 2000, Jeong and Jang, 2000). The validation approach used in these experimental studies is incomplete due to the reliance on monopole sources from out-of-plane pencil-lead breaks or ball drops on the plate surface. In this work, we obtained the AE signals in plate samples by finite-element modeling (FEM), and the sources of these signals include realistic dipoles as well as the important variable of source depth. The modeled signals also have the advantage that the exact three-dimensional source location is known. Thus, WT-based signal-arrival times at different propagation distances can be quantitatively evaluated for their correspondence to a single group velocity.

2. Signal Database and Wavelet Transform

An AE signal database of plate top surface out-of-plane displacement as a function of time at three propagation distances was used. The AE signal database, specimen geometry and the relevant WT information were described in detail in Part 1 (Hamstad et al., 2002) of this two-part paper. Hence, we have not repeated that description here.

3. WT−Based Source Location (Large Plates)

The extraction of arrival times from the WTs of AE signals was successively examined by several approaches. The first approach was based on the results of a WT of the simulated wideband AE signals that had been filtered with a 40 kHz high-pass filter. In this case, the information extracted from the WT result consisted of data pairs of arrival time and frequency based upon absolute peaks of the WT's magnitude (WT coefficient). When sets of such data pairs were compared for three different propagation distances from a given AE source, it was deter-

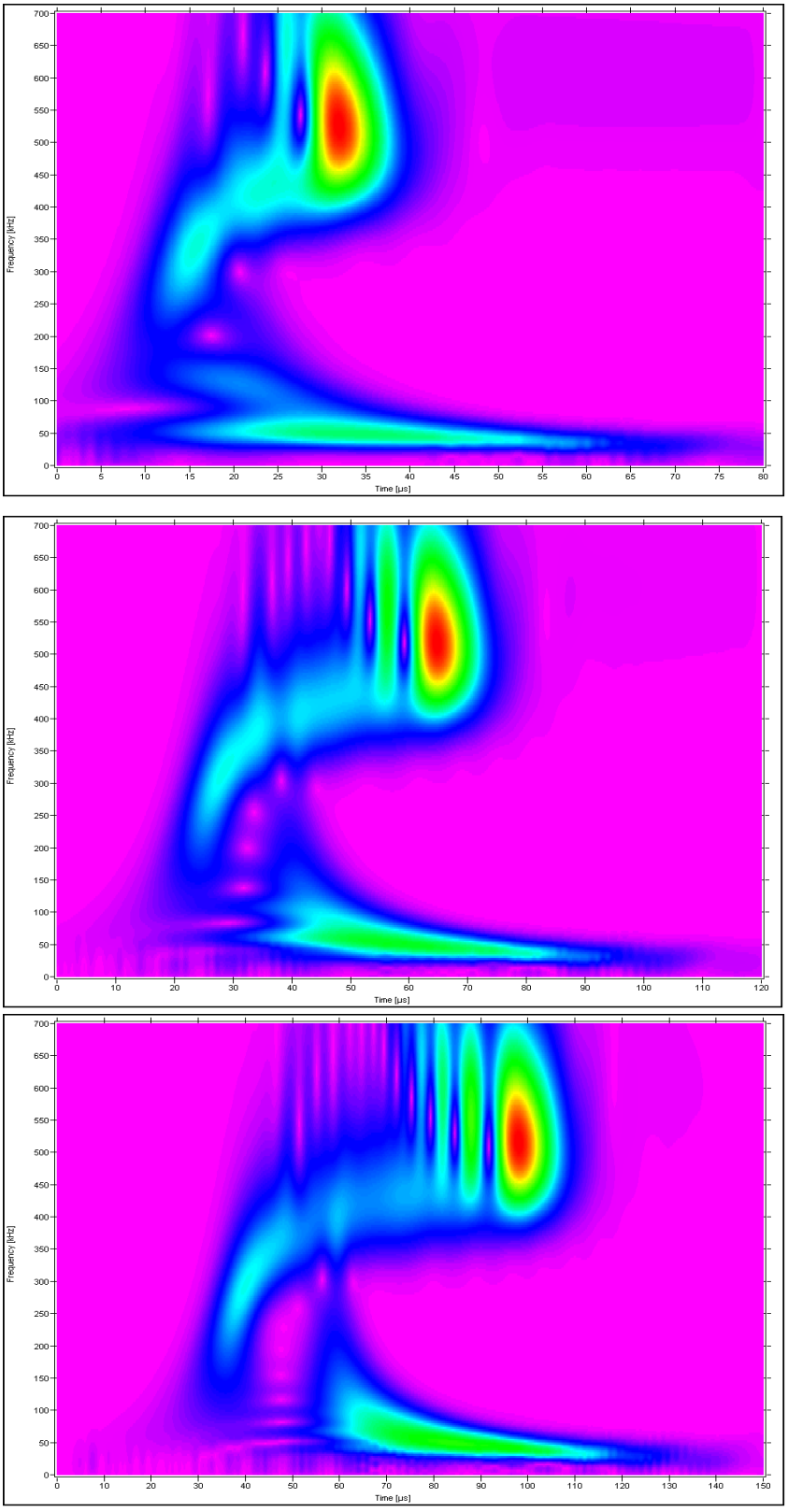

Fig. 1 WT plots used to determine AE signal arrival times from the peak WT magnitudes of the So mode at 522 kHz. The AE source was an in-plane dipole at a depth of 2.037 mm with propagation distances of (a) 60 mm, (b) 120 mm, and (c) 180 mm. AE signals filtered with 40 kHz high pass filter prior to WT. Frequency (0 to 1 MHz) versus time (a: 0 to 80 µs, b: 0 to 120 µs, and c: 0 to 150 µs from top to bottom).

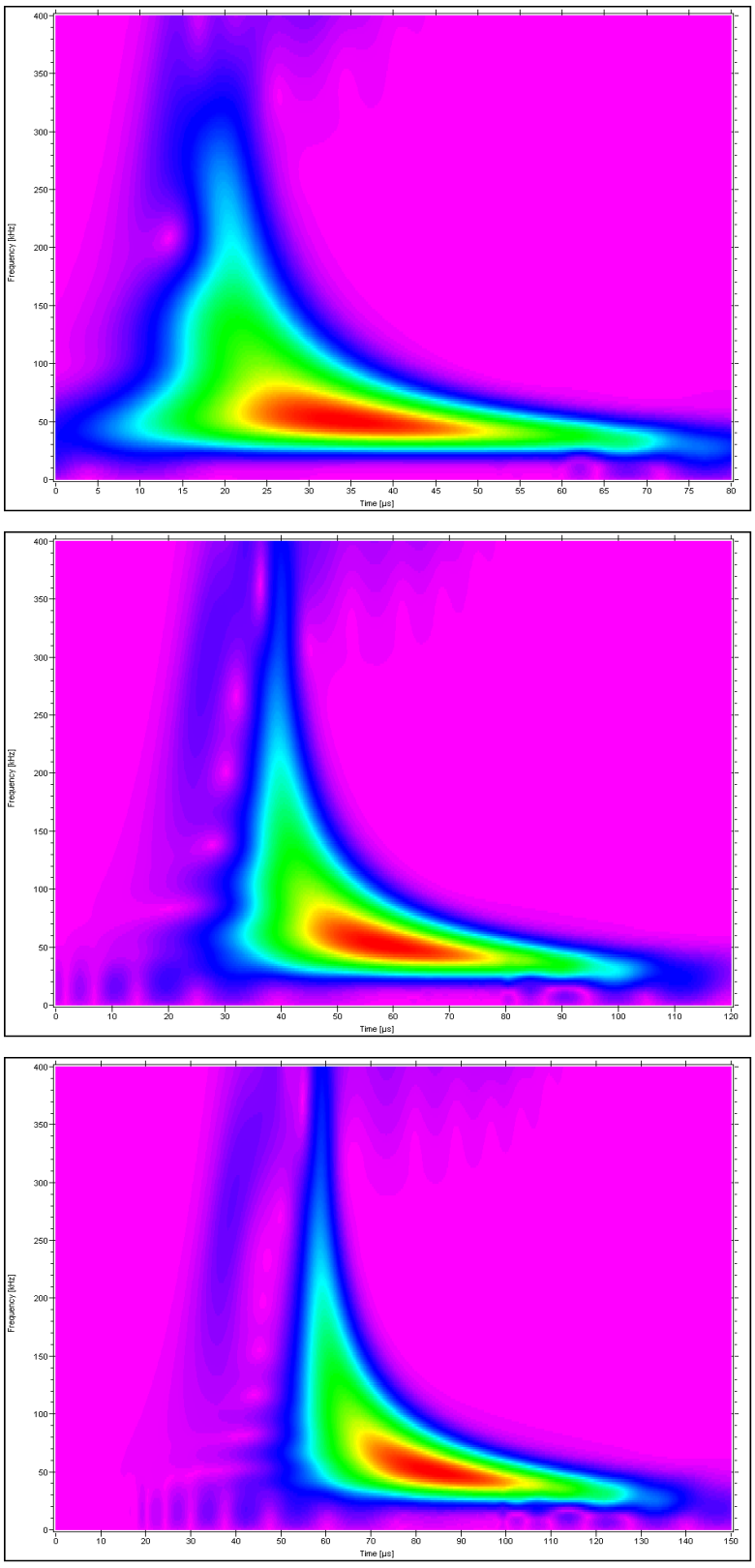

Fig. 2 WT plots used to determine AE signal arrival times from the peak WT magnitudes the Ao mode at 66 kHz. The AE source was an in-plane dipole at a depth of 0.783 mm. The propagation distances and filter were the same as for Fig. 1(a), (b), and (c). Frequency (0 to 400 kHz) versus time (same scales as Fig. 1; 1 MHz vs. a: 80 µs, b: 120 µs, and c: 150 µs top to bottom).

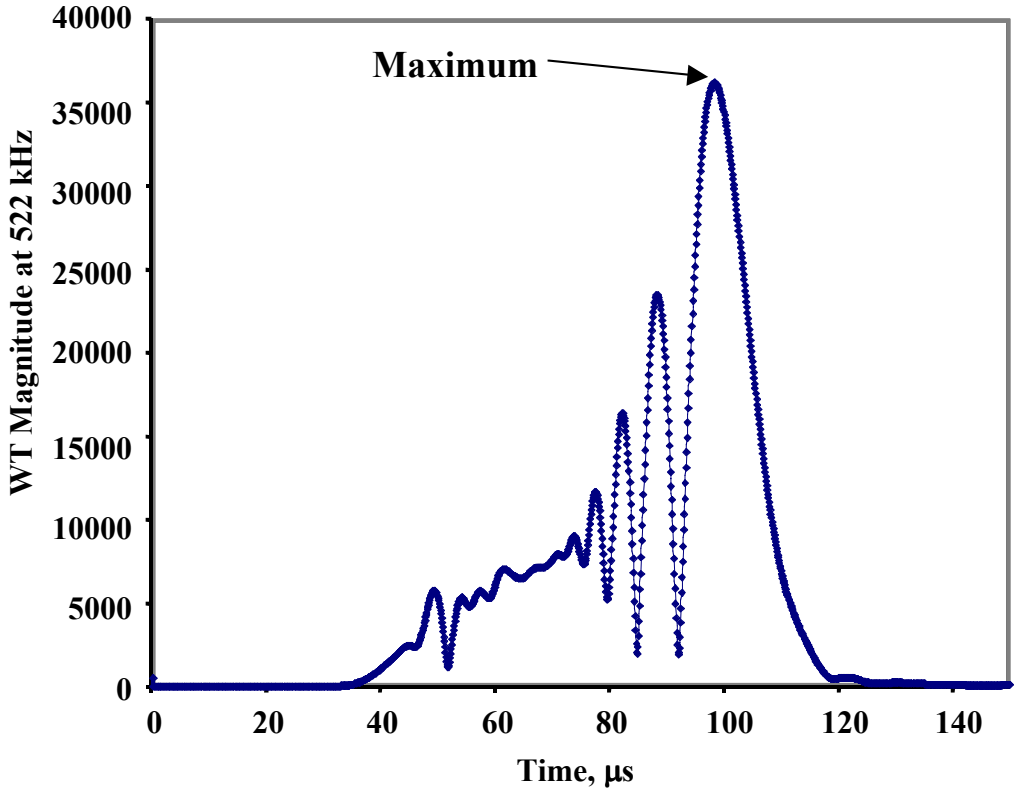

Fig. 3 Example of the WT magnitude versus time for the So mode at 522 kHz from the WT result shown in Fig. 1(c). Plot illustrates the determination of the arrival time of the peak magnitude near the selected group velocity of the mode.

mined that there were differences in the frequency values of the maximum magnitude as a function of propagation distance. Since determining arrival times at different frequencies and thus different group velocities at each sensor would complicate the process of source location, it seemed best to examine alternative approaches so that the simplest use of WT data to extract arrival times could be developed.

The second approach that was examined was based upon choosing a single frequency for a particular fundamental Lamb symmetric (So) or anti-symmetric (Ao) mode. Based upon the modal region of the WT that had a large magnitude, a single frequency was chosen in the same fashion as the source-identification approach in Part 1 (Hamstad et al., 2002). Then, using this frequency, the arrival time of the maximum magnitude of the WT at that frequency (and associated mode) was determined, as was done by Yamada et al. (2000). It was found that choosing the parameters of the WT to enhance the resolution and smoothness (as discussed in Part 1: Hamstad et al., 2002) of the WT result was important to facilitate the determination of the maximum at the selected frequency and mode. To initially examine this approach in more depth, two different in-plane dipole source cases were chosen. In one case the source depth was chosen such that the maximum magnitudes of the WT were in the lower-frequency regime of the fundamental anti-symmetric mode. In the other source-depth case, the maximum magnitudes of the WT were in the higher-frequency regime of the fundamental symmetrical mode. Table 1 shows the arrival times obtained at the indicated frequencies and modes (Ao, 66 kHz and So, 522 kHz) for the three available propagation distances (60, 120, 180 mm). In contrast to Part 1, a higher frequency was used for Ao to be more certain that the arrival times would not be altered by the 40 kHz high-pass filter. Figures 1 and 2 show the high-resolution WT results, which were used in the two cases. The WT-parameters used were Wavelet size (WS) = 600 samples, Maximum Fre-

Table 1. Arrival times (μs) of the peak WT magnitude for in-plane dipole source signals filtered with a 40 kHz high-pass filter in the large plate.

So mode at 522 kHz						Ao mode at 66 kHz				
Source	Distance, mm			Velocity, mm/μs		Distance, mm			Velocity, mm/μs	
depth, mm	60	120	180	Slope	Theoretical	60	120	180	Slope	Theoretical
2.037	31.9	64.6	98	1.82	1.78	-	-	-	-	-
0.783	-	-	-	-	-	29.1	51.9	75.1	2.61	2.61

quency (MF) = 700 kHz, Frequency Resolution (FR) = 3 kHz for the signal dominated by the So mode and WS = 600 samples, MF = 400 kHz, FR = 2 kHz for the signal dominated by the Ao mode. The sources were at depths of 2.037 mm (Fig. 1 for the dominant symmetric mode) and 0.783 mm (Fig. 2 for the dominant anti-symmetric mode). Figure 3 shows a plot of the WT magnitude as a function of time at a single frequency of 522 kHz for the 180 mm distance case of Fig. 1. The time of arrival of the maximum WT magnitude for the selected mode and frequency was obtained from the available spreadsheet that gives the WT magnitude (WT coefficient) as a function of time and frequency. The time resolution of the spreadsheet was 0.1 μs, which is the same resolution as the re-sampled simulated AE signal. Since the exact locations of the source and sensors are known, the information in Table 1 can be plotted to form distance-versus-time plots. The slopes of these plots provide group velocities as well as coefficients of determination (R^2) for the straight line fits. Table 1 shows these slope-based group velocities as well as the group velocity (for the mode and frequency) available from the relevant theoretical dispersion curves. Figure 4 shows an example of one of the plots (for the Fig. 1 case, 2.037 mm source depth) of distance versus arrival time along with the equation that describes the straight-line fit. The plot (not shown) of the other case (0.783 mm depth) gave a similar straight-line fit. The excellent straight-line fits imply that the arrival times correspond very closely to a single group velocity that is quite near the theoretical group velocity.

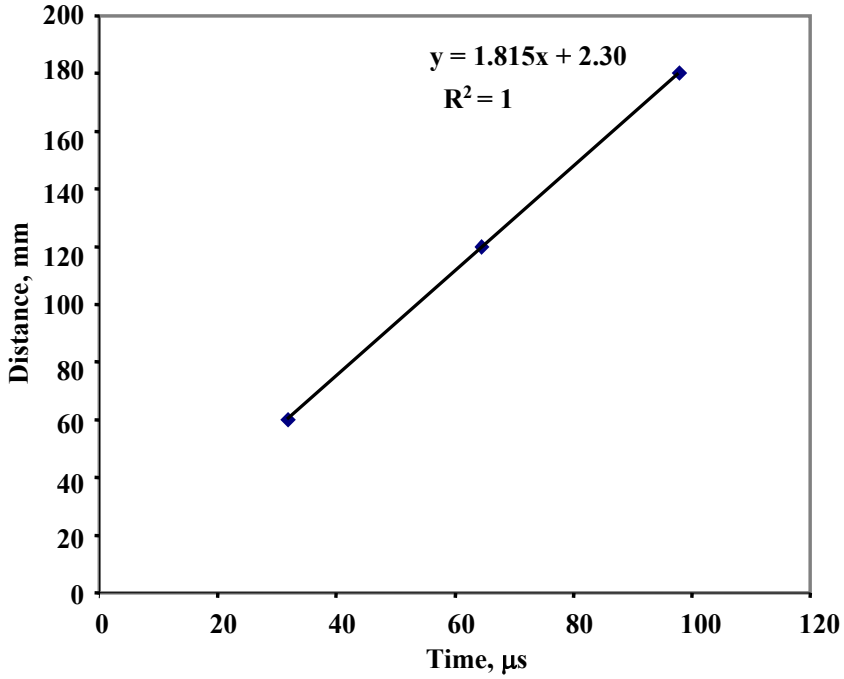

Fig. 4. Plot of propagation distances versus arrival time of peak magnitude of the So mode at 522 kHz for the WTs in Fig. 1. Equation of straight-line fit with slope of 1.815 mm/μs representing the slope-based group velocity. $R^2 = 1$, correlation coefficient.

Table 2. Arrival times (μs) of the peak WT magnitude for in-plane dipole source signals filtered with a 100 to 300 kHz bandpass in the large plate.

Source	Distance, mm			Velocity, mm/μs		Distance, mm			Velocity, mm/μs	
depth, mm	60	120	180	Slope	Theoretical	60	120	180	Slope	Theoretical
2.037	15.9	28.2	40.5	4.88	4.88	-	-	-	-	-
0.783	-	-	-	-	-	25.2	45.7	65.7	2.96	3.00

It is worthwhile to point out that the straight-line fit has an intercept that does not pass through the source origin (even with an excellent fit, $R^2 = 1$, of the data to a straight line). The reason for this behavior is likely due to the fact that the wave propagation needs to progress over some number of plate thicknesses in order to fully develop the Lamb modes at their propagation velocity. We also note that the group velocities determined from the WTs of the finite element data did not always correspond exactly to those determined from the theoretical group velocity (dispersion) curves. For example, when the arrival times used to calculate the indicated velocity in Table 1 of Part 1 (Hamstad et al., 2002) were used along with the propagation distances to obtain a plot of distance versus time the slope-based group velocity was 2.45 mm/μs. This value is 1.2 % faster than the dispersion curve velocity of 2.42 mm/μs for the Ao mode at 50 kHz. As will be seen later in the description of a proposed source location procedure, we suggest the group velocities determined from WT results might be expected to provide more accurate results. But the correctness of this assumption will need to be determined through additional research.

A third approach was also examined. This approach was really just a deviation of the second one. In this case the modification was to filter the FEM-based signals with a 100 to 300 kHz bandpass filter before calculating the WTs. This frequency range was chosen since it has often been used in experimental AE applications. Figure 5 (Fig. 1 case) and Figure 6 (Fig. 2 case) show the resulting high-resolution WT results for the same two sources. These WT results were calculated for the filtered signals, which are also shown in Figs. 5 and 6. The WT-parameters used were WS = 600 samples, FR = 2 kHz, and MF = 400 kHz. In this case the maximum magnitudes of the WTs are in a different frequency range. Table 2 shows the selected frequencies and modes (Ao, 134 kHz and So, 262 kHz) for each case as well as the arrival times determined from the WTs; also shown are the group velocities from the plots of distance versus time and the group velocities from the dispersive group-velocity curves at the selected frequencies and modes. The slope-based group velocities shown in Table 2, again, were quite close to those obtained from dispersion curves. As before, the plots of distance versus arrival time had excellent fits but again did not pass through the origin, presumably due to the need to propagate several plate thicknesses to develop the Lamb modes and their group velocities. Thus, in this range of bandpass frequency, the arrival times correspond very closely to a single group velocity very near the theoretical velocity.

4. Proposed Method of WT-Based Source Location for Experimental Data (Large Plate)

The results above indicate that the approach of using a fixed frequency of an energetic mode to determine an arrival time at the maximum magnitude of a WT (Yamada et al., 2000) could result in accurate arrival times that are associated with a particular wave mode and corresponding group velocity. But, since the calculated group velocities from the finite-element data did not always correspond exactly to the dispersion-curve values, it may be useful to account for this aspect. By providing for this aspect, it may be possible to obtain the best possible experimental location accuracy with a WT-based technique. The approach we suggest would use the group

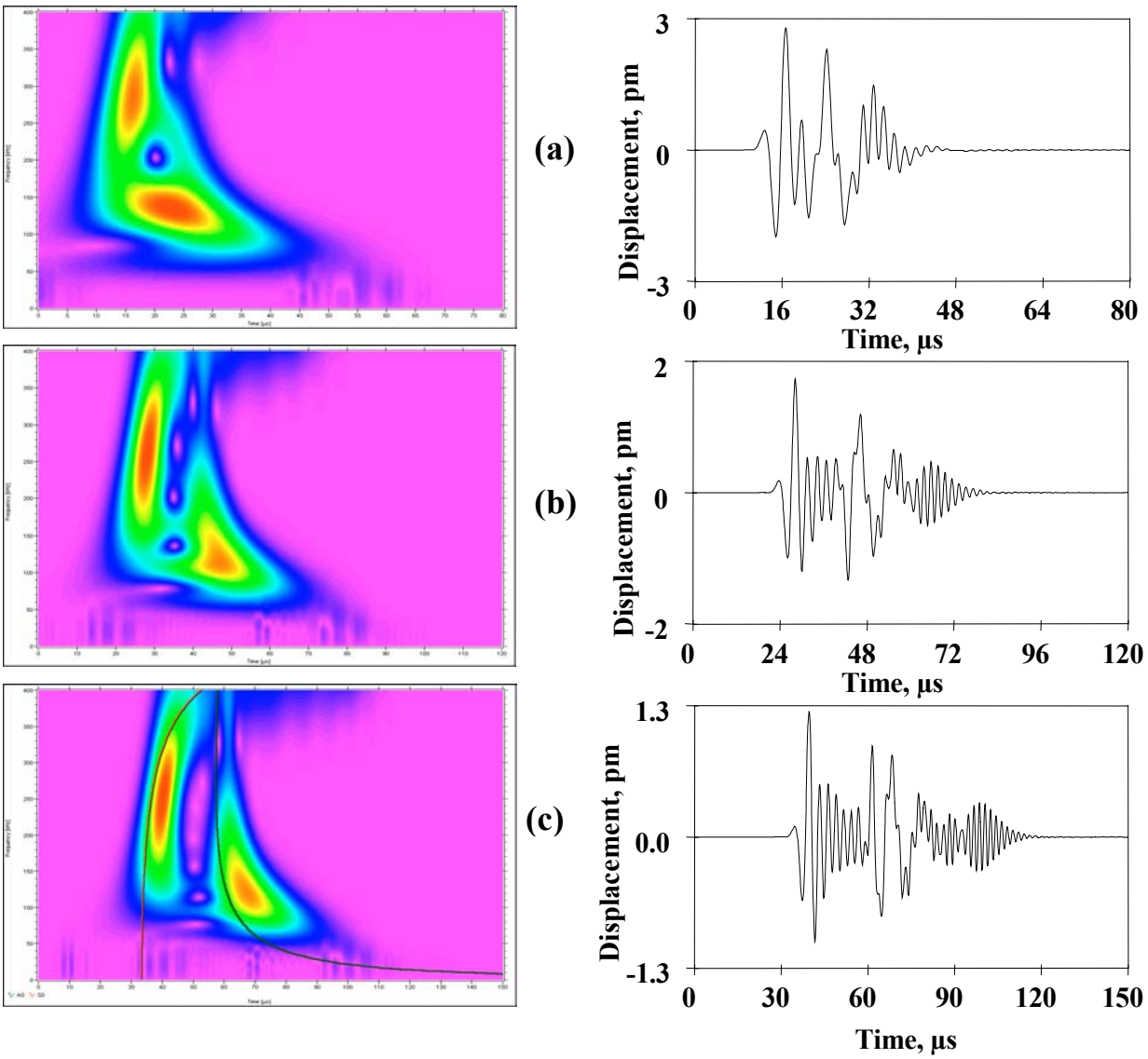

Fig. 5 WT results (frequency 0 to 400 kHz versus time (0 to 80, 0 to 120, and 0 to 150 µs)) for the same cases shown in Fig. 1 but with a 100 to 300 kHz bandpass filter prior to calculating the WT. Fig. 5(c) also shows superimposed Ao and So group-velocity-based dispersion curves after conversion to arrival times based on the propagation distance of 180 mm. Also shown are the corresponding filtered AE signals.

velocity from the dispersion-based curves as an initial group-velocity estimate. Possibly a better group-velocity value could be determined as described below by pre-experiments. The pre-experiment approach would replace that illustrated in Fig. 4 since the propagation distances used to construct that figure are available only for the FEM data. We point out that the "calibrated" group velocity extracted from Fig. 4 could be viewed as compensating for small differences in group velocity (compared to dispersion-based values) induced by the WT algorithm. Presumably these algorithm-induced differences would be a part of each WT calculation with a particular algorithm. Also, the pre-experiments would be necessary when accurate group velocities cannot be calculated.

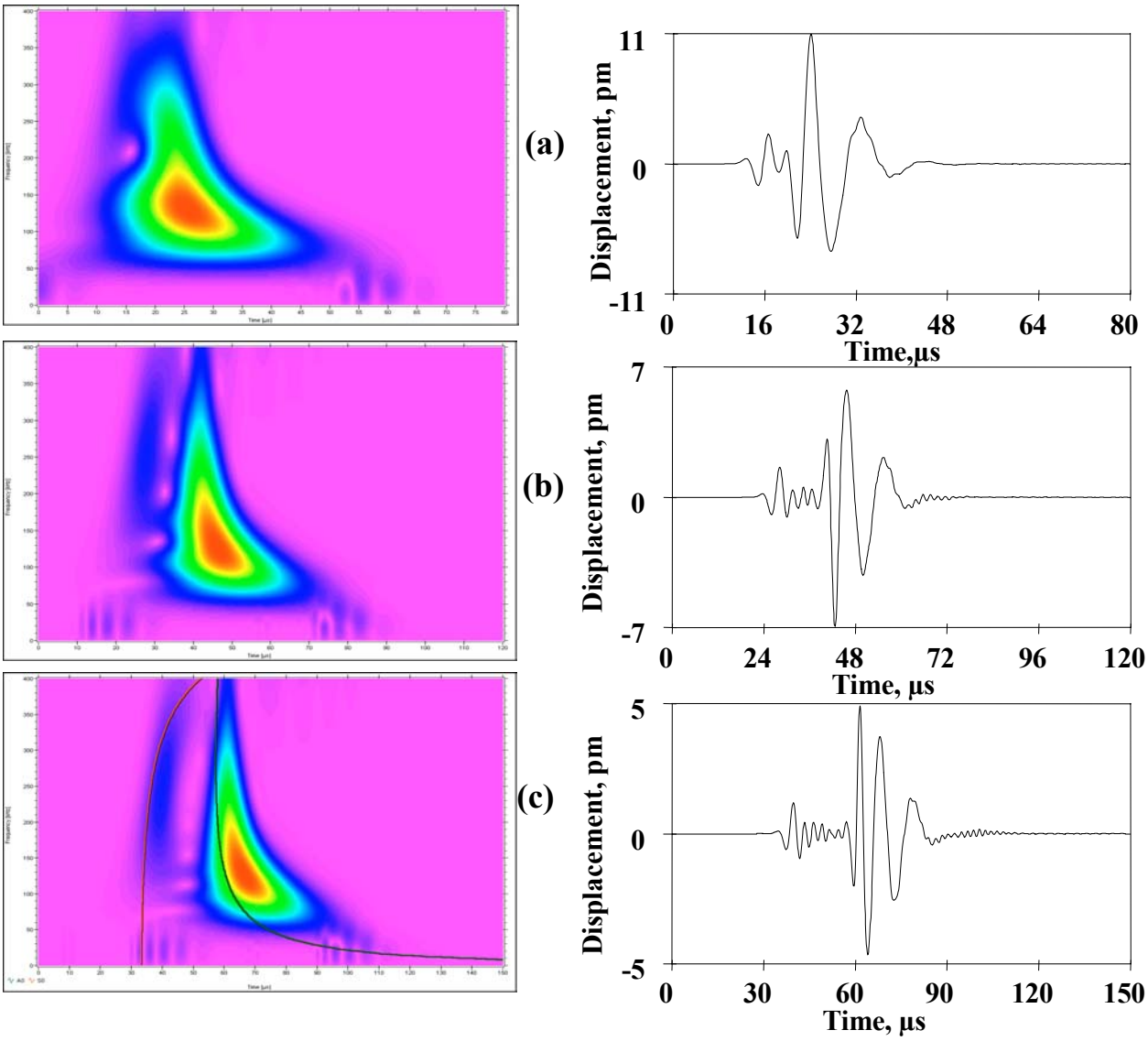

Fig. 6 WT results (same scales as Fig. 5) for the same cases shown in Fig. 2 but with a 100 to 300 kHz bandpass filter prior to calculating the WT. Fig. 6(c) shows the superimposed Ao and So group-velocity-based dispersion curves after conversion to arrival times based on the propagation distance of 180 mm. Also shown are the corresponding filtered AE signals.

5. Comments Relative to the Location Approach for Real AE Signals

With actual AE data, in particular narrow-band data, the preliminary task of selecting the wave mode to associate with the WT maximum magnitude region may require some pre-experiments. The purpose of conducting pre-experiments with pencil lead breaks and the real sensors would be to identify the mode(s) associated with the peak magnitude frequency range(s) of the WT and to determine corresponding WT-based group velocities. A large plate of the same thickness and material could be used for these pre-experiments. Good control of the position and force direction of the lead break is necessary. But in principle, an in-plane pencil break on the plate edge close to the top or bottom surfaces would allow identification of the dominant-energy WT frequencies for the anti-symmetric modes (typically for thin plates this will be the fundamental anti-symmetric mode). And an in-plane lead break located almost exactly at the mid-

plane could allow (with careful filtering) the determination of the dominant frequencies of the peak-magnitude region of the WT for the symmetric modes (typically for thin plates this is expected to be the fundamental symmetric mode). These frequencies and modes could then be used with dispersion-based group-velocity curves to provide the initial estimates of the group velocities to be used to calculate the source location. In addition WTs from sensors at several accurately known distances from these experimental sources could be used to obtain "calibrated" group velocities (as referred to above).

In contrast to the source-identification task with a subset of WT data, the dependence of the WT results on source depth does not cause significant problems in determining source location. It is necessary only to add a step in the calculation of source location that determines which mode is dominant in an AE signal by calculating appropriate Ao/So ratios as described in Part 1 (Hamstad et al., 2002). Based on the ratio determined, the most energetic mode and associated frequency can be used to extract the WT-based arrival times. Also, the correct group velocity for the dominant mode and frequency for each AE signal can be selected for the calculation of the source location.

6. Effects of Electronic Noise

In experimental cases, the AE signal is a combination of signal (from the AE source) and noise (from the electronics). Thus, to be useful, the above method of WT-based source location must retain its determination of accurate arrival times for a single group velocity in the case of experimental signals that combine signal and noise. To examine this issue we added electronic noise to the calculated FEM signals and studied the WT-based determination of arrival times. The study was carried out as a function of the signal-to-noise (S/N) ratio.

The noise signals were taken from two different wideband sensor/preamplifier combinations. These experimental signals were obtained with the wideband sensors coupled only to air. In addition, the sensors were protected from any possible laboratory airborne signals. Prior to being added to the FEM calculated signals, the noise signals were filtered with a six-pole digital Butterworth filter from 40 kHz to 1.2 MHz. As Fig. 7 shows, the typical spectra of the noise signals were considerably different from each other. In one case the electronic noise increases significantly with decreasing frequency. In the other case, the electronic noise amplitude is distributed more uniformly with frequency, with a peak region near the middle of the frequency range. By using noise signals with these two different spectrums, we attempted to broaden the results of the study.

Also to broaden the results of the study, two distinctly different FEM calculated signals were selected. In one case, a higher-frequency region of the fundamental symmetric mode dominated the AE signal energy. In the second case, a lower-frequency region of the fundamental anti-symmetric mode dominated the AE signal energy. The source for both signals was an in-plane dipole located at 180 mm from the sensor. In the case of the dominant symmetric mode the source was at a depth of 2.35 mm (mid-plane). The dominant anti-symmetric-mode source was at a depth of 0.47 mm below the top surface of the large plate.

In order to quantitatively characterize the S/N ratio, the peak amplitudes of the noise and the calculated AE signals (40 kHz high-pass) were determined over the 150 μs portion of each signal used in the WTs. Then the noise signals were multiplied by appropriate factors to obtain the desired range of S/N ratios, based on the peak amplitudes.

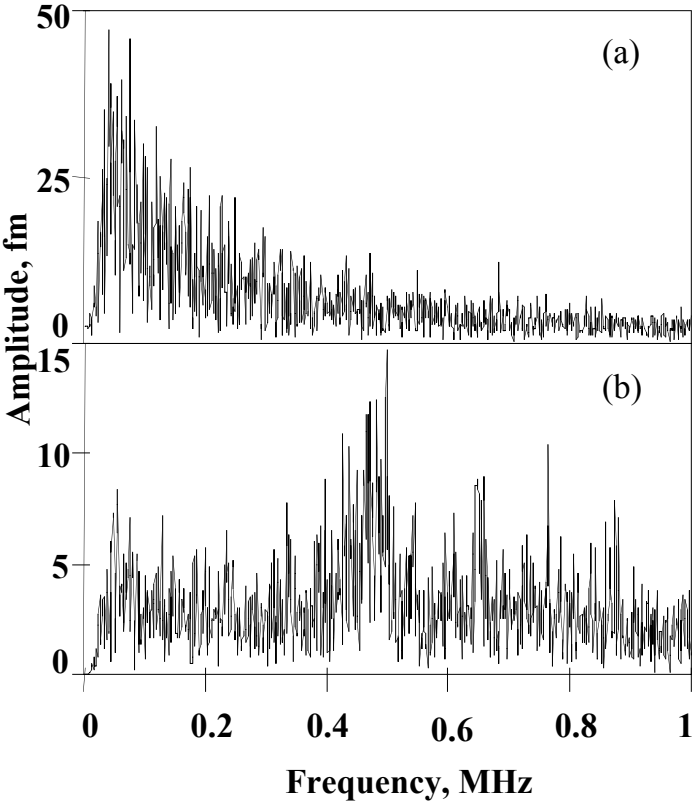

Fig. 7 Typical frequency spectra for the two experimental noise signals calculated from an 819.2 μs signal length. Low-frequency emphasis (a) and distributed frequencies (b).

Figure 8 shows the WTs of the two calculated AE signals ((a) and (b) without added noise) and the two noise signals ((c) and (d)). These WTs were calculated with the following high-resolution parameters (WS = 600, FR = 3 kHz [0-600 kHz case] and 2 kHz [0-400 kHz case]). Following the approach used earlier in this paper, the arrival times of the peak magnitudes of the WTs were determined at 522 kHz (AE signals dominated by the symmetric mode) and at 66 kHz (AE signals dominated by the anti-symmetric mode). Table 3 shows the determined arrival times at 522 kHz for the two different noise types at the selected S/N ratios. Table 4 shows the arrival times at 66 kHz for the two noise cases. No arrival times are shown in the tables when the peak magnitude of the WTs was not obvious. In all cases the WTs were calculated with the high-resolution parameters used to produce Fig. 8.

Table 3. Arrival times (μs) determined from the peak WT magnitude at 522 kHz for the original AE signal dominated by a higher-frequency region of the fundamental symmetric mode.

S/N ratio	Noise dominated by low frequencies	Noise with distributed frequencies
no noise	97.9	97.9
10:1	97.9	97.9
5:1	97.9	97.9
2:1	97.9	97.9
1:1	97.9	97.8
1:2	97.9	87.8
1:5	101.8	117.2
1:10	101.8	–
Noise signal	33.1, 101.5	115.9, 15.5

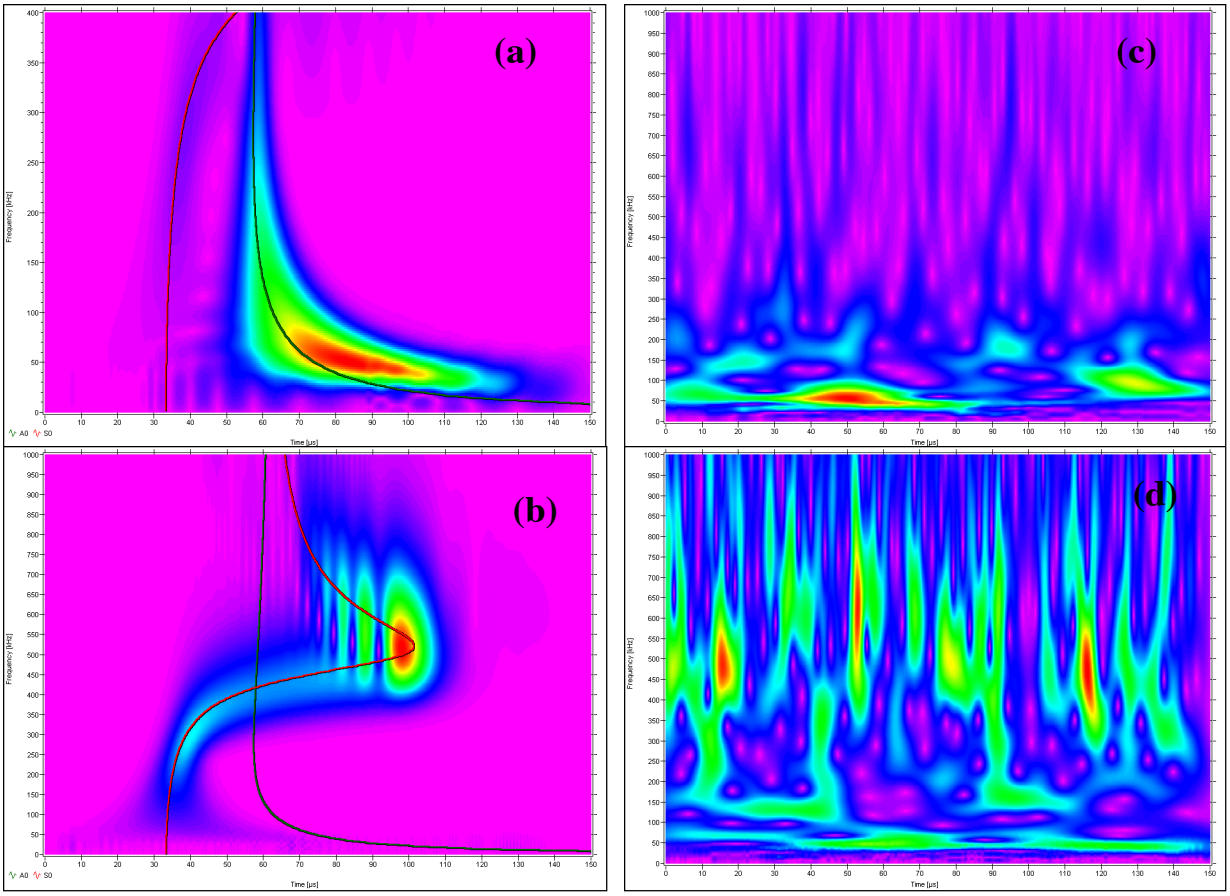

Fig. 8 WTs of the calculated AE signals and the experimental electronic noise for 150 μs length signals: (a) for AE signal at 180 mm propagation distance with dominant fundamental anti-symmetric mode; (b) for AE signal at 180 mm propagation distance with dominant fundamental symmetric mode; (c) for electronic noise with low-frequency emphasis; and (d) for electronic noise with distributed-frequency emphasis.

Table 4. Arrival times (μs) determined from the peak WT magnitude at 66 kHz for the original AE signal dominated by a lower frequency region of the fundamental antisymmetric mode.

S/N ratio	Noise dominated by low frequencies	Noise with distributed frequencies
no noise	75.1	75.1
10:1	75.6	75.2
5:1	76.1	75.3
2:1	77.1	75.6
1:1	80.3	76.1
1:2	47.7	76.2
1:5	–	74.6
1:10	–	26.7
Noise signal	49.2	66.6, 24.4

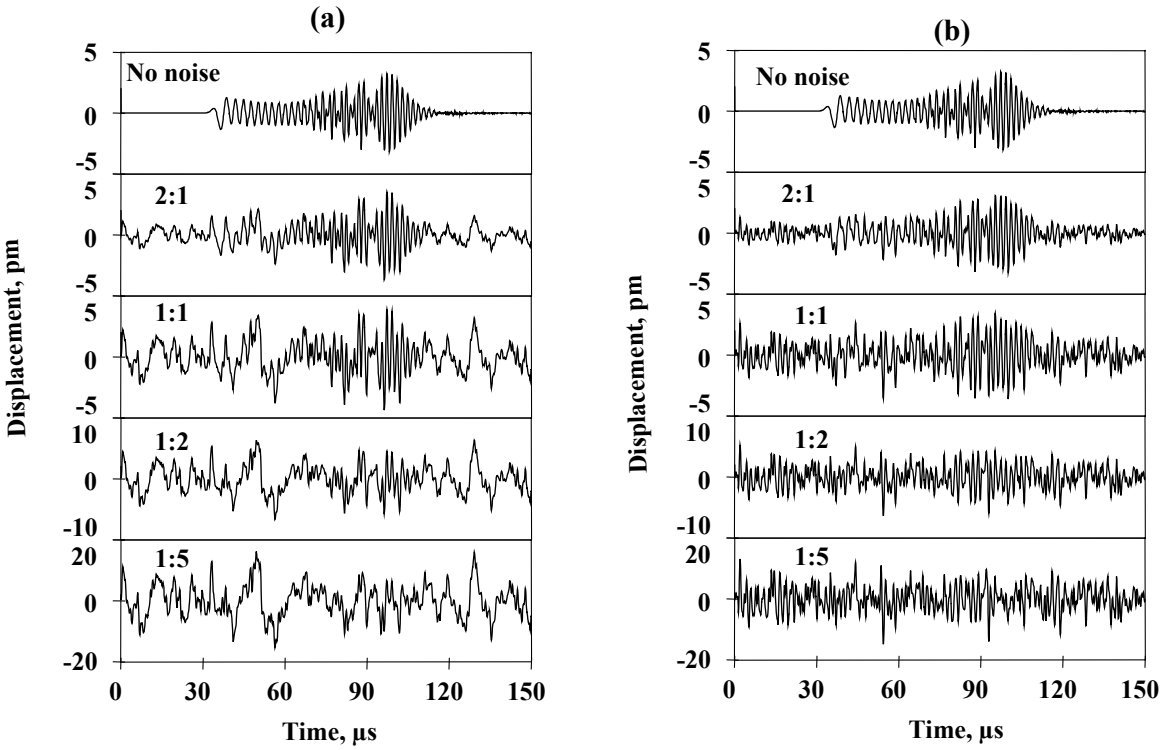

Fig. 9 Waveforms of signal-plus-noise at the indicated S/N ratios for the AE signal at 180 mm propagation distance dominated by the fundamental symmetric mode: (a) noise with low-frequency emphasis; (b) noise with distributed-frequency emphasis.

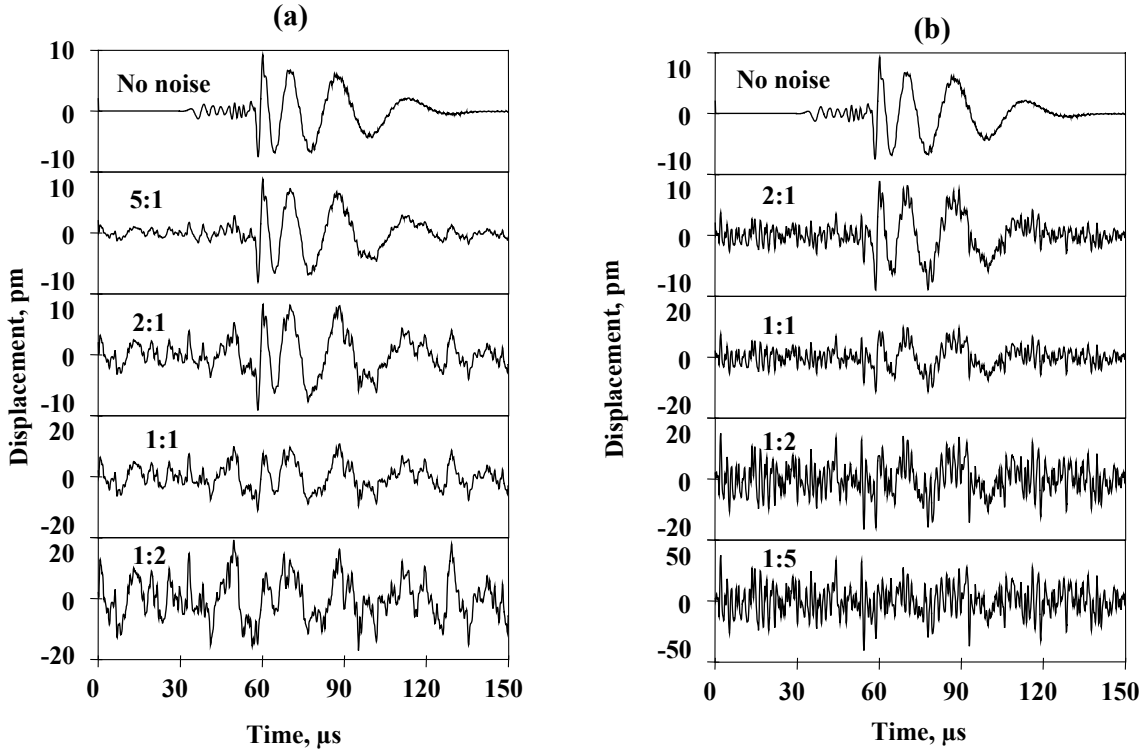

Fig. 10 Same types of waveforms as Fig. 9 for the AE signal at 180 mm propagation distance dominated by the fundamental anti-symmetric mode.

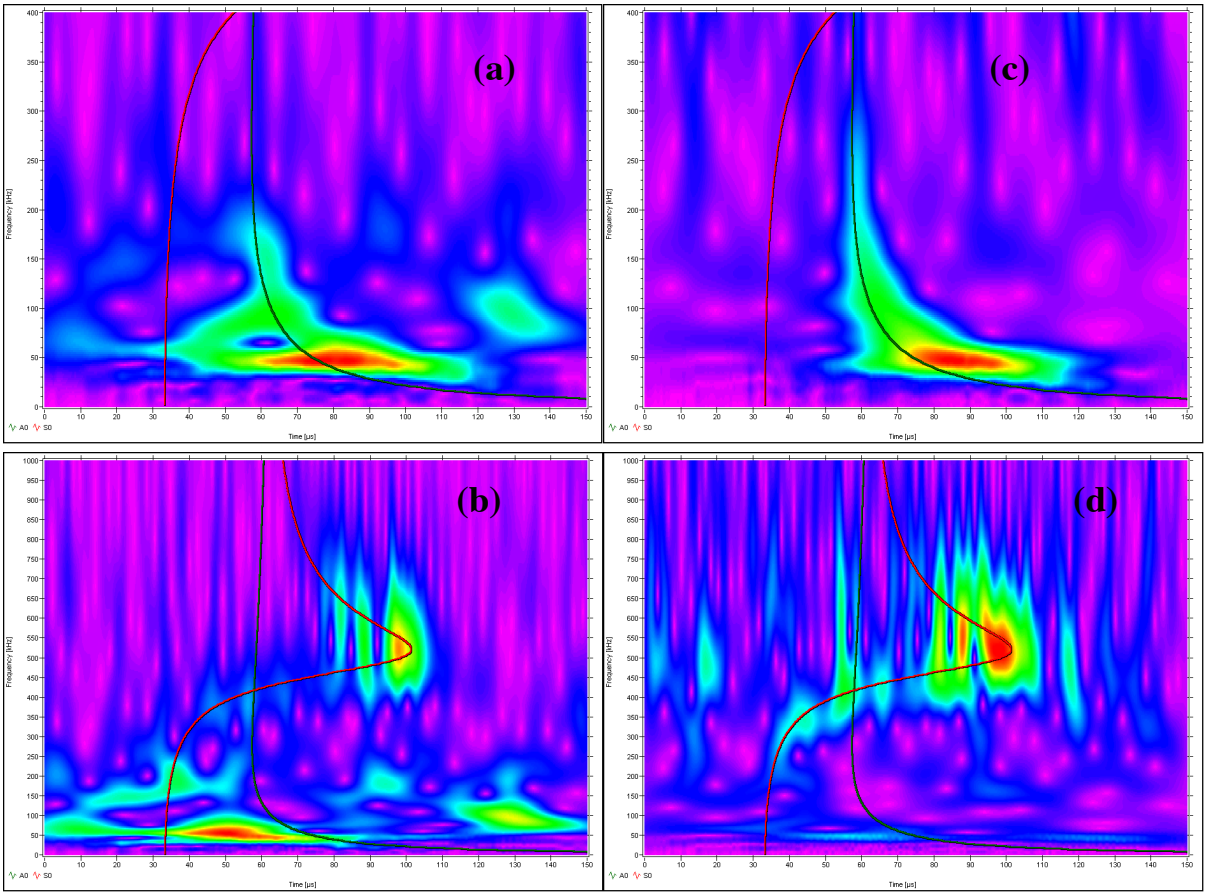

Fig. 11 WTs of waveforms of signal plus noise. Signals at 180 mm from the in-plane dipole source. The noise in (a) and (b) was dominated by low frequencies and in (c) and (d) by distributed frequencies. The signal in (a) and (c) was dominated by the fundamental anti-symmetric mode from the source at a depth of 0.47 mm. In (b) and (d) the signal was dominated by the fundamental symmetric mode from the source at a depth of 2.35 mm. The signal-to-noise ratio in each case was 1:1.

To provide a clearer understanding of the results in Tables 3 and 4, Fig. 9 shows selected waveforms of signal-plus-noise for the two noise cases when the original AE signal was dominated by a higher-frequency region of the symmetric mode. Figure 10 shows the same type of selected results when a lower-frequency region of the anti-symmetric mode dominated the original AE signal. Examination of the above figures and tables reveals several key aspects about the effects of electronic noise on the WT-determination of arrival times from a particular mode and frequency. First, when the S/N ratio becomes too small, the arrival time of the WT magnitude peak typically moves toward the WT peak magnitude of the noise signal (at the selected frequency). Second, even with a relatively poor S/N ratio of 1:1 as shown in Figs. 9 and 10, the WT-based arrival time is still reasonably accurate. As Figs. 9 and 10 show for these cases, it is becoming difficult to extract by eye the AE signal. And clearly, a threshold-based technique would lead to inaccurate arrival times (or no hit detected) not associated with a known group velocity. The worst result at this 1:1 ratio is the case of the signal dominated by the low-frequency anti-symmetric mode and the noise dominated by low frequencies. Since WTs result in better time resolution at higher frequencies, it is possible that the slightly poorer accuracy at 66 kHz is due to the characteristics of the WT. More likely, the result is due to the frequency peaks of the original AE signal and the noise being in the same frequency range. This conclusion

is based on the observation (see Tables 3 and 4) that errors in the arrival times appear at higher S/N ratios when the noise and original signals have peaks in the same frequency region.

The reason why reasonably accurate arrival times can be extracted from the WT results at S/N ratios of 1:1 or less seems to be due to the fact that the WT spreads out the noise over the bandpass frequency range while preserving the spread of the noise in time. Determinations of arrival times by penetration of a fixed threshold have the noise spread out only in time. Thus, such approaches typically cannot even detect an AE hit at S/N ratios as low as 1:1. Figure 11 demonstrates at a S/N ratio of 1:1 that the WT of the AE signal plus noise is dominated in all four cases by the same WT region that dominated when only the AE signal was present (compare Fig. 11 with Figs. 8(a) and 8(b)). In Fig. 11 the four cases of AE signal plus noise are: (a) low-frequency noise and low-frequency AE signal; (b) low-frequency noise and high-frequency AE signal; (c) distributed noise and low-frequency AE signal; (d) distributed noise and high-frequency AE signal.

We did not investigate the narrow-band S/N ratio case, since we did not have available the digital displacement calibration of a typical 150 kHz resonant commercial AE sensor. Thus, we could not properly alter the calculated sensor signal for the AE source to correspond to the sensor resonance. We expect that the above WT-based method of detection of arrival times would not be as robust at low S/N ratios, since both the AE signal and the noise would be concentrated in the same relatively narrow frequency range.

An additional positive of the WT-based method, in the case of wideband waveform-based AE measurement systems, may be that fewer AE events would have only one useable hit. If the measurement system were configured so that all the waveforms from a group of sensors were recorded when one sensor was hit (i.e. a signal above the threshold), then WT-based processing could extract relevant arrival times from the sensor channels where threshold-penetration hits would not occur. Thus, signal arrival times corresponding to a single group velocity could be extracted from the channels where the AE signal had attenuated into the background electronic noise. And potentially a source location could be calculated for an event where it could not be calculated with a threshold-based AE system.

7. WT for Source Location in Samples with Nearby Edges

When the lateral size of the test specimen is decreased so that nearby edges are present, the AE signals and their WTs become much more complicated. This result was illustrated in Part 1 (Hamstad et al., 2002) in Figs. 16 and 17. Since the distribution of WT-illustrated signal energy in these figures does not clearly follow the shapes of the superimposed fundamental Lamb-mode curves from the dispersion relations, the use of the approaches developed for source location in the large plate might be expected to experience difficulties for the coupon specimen. Further, since the distortion of the WT results is due to edge reflections, moving the source from side-to-side across the 25.4 mm width of the coupon specimen will change the reflections and WTs as was illustrated in Fig. 18 of Part 1 (Hamstad et al., 2002). The current coupon database, except for the case illustrated in Fig. 18 of Part 1 (Hamstad et al., 2002), does not include the side-to-side variation of the source position.

In spite of the limited database (side-to-side source position), we examined for the coupon specimen the application of the techniques applied to the large-plate signals. The results of this examination in the coupon (using 40 kHz high-pass signals) for the same source cases used in the

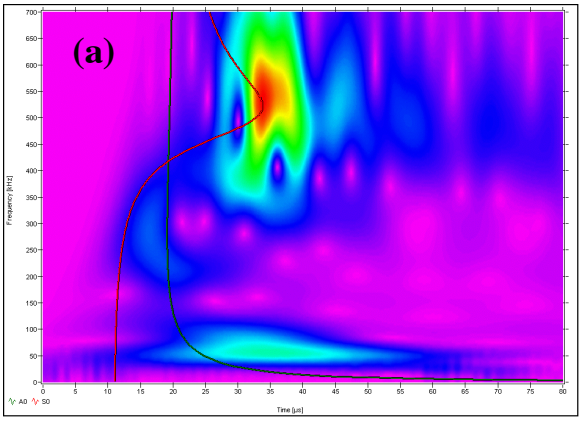

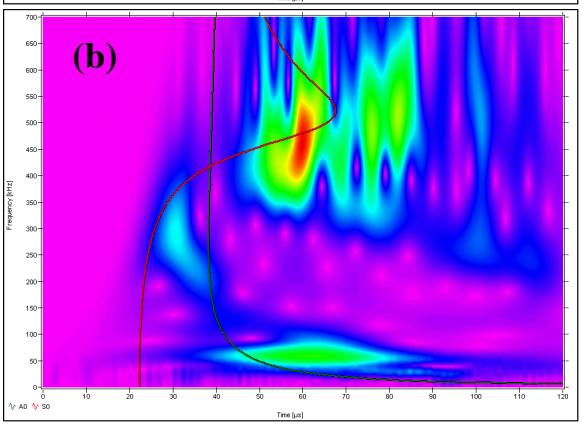

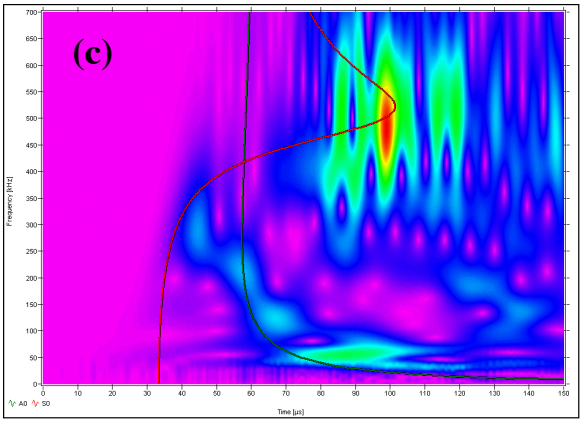

Fig. 12 WT plots used to determine AE signal arrival times from the peak magnitudes of the So mode at 522 kHz for the coupon specimen. The AE source was an in-plane dipole at a depth of 2.037 mm with propagation distances of (a) 60 mm, (b) 120 mm, and (c) 180 mm. AE signals filtered with 40 kHz high-pass filter prior to WT. Frequency (0 to 700 kHz) vs. time (0 to 80, 0 to 120, 0 to 180 μs from top to bottom). Superimposed group velocity curves of fundamental modes.

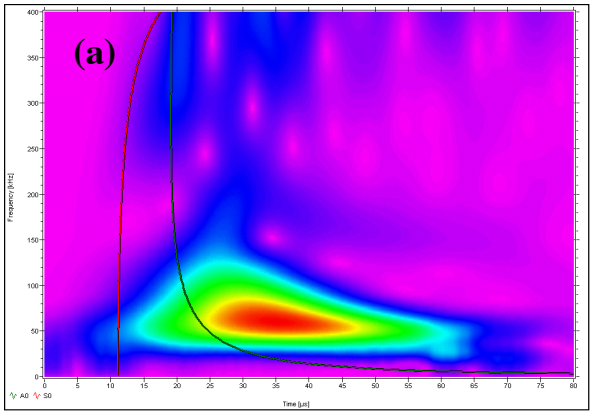

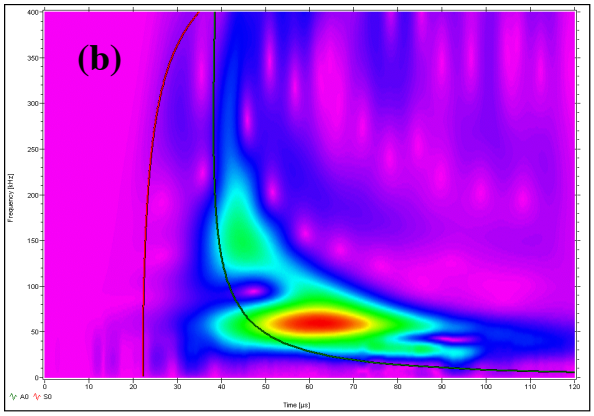

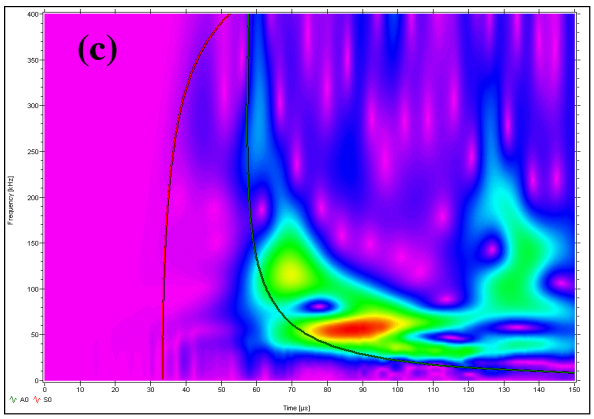

Fig. 13 WT plots used to determine AE signal arrival times from the peak magnitudes of the Ao mode at 66 kHz for the coupon specimen. The AE source was an in-plane dipole at a depth of 0.783 mm. The propagation distances and filter were the same as for Fig. 12 (a), (b), and (c). Frequency (0 to 400 kHz) versus time (same scales as Fig. 12, top to bottom).

Table 5. Arrival times (μs) of the peak WT magnitude for in-plane dipole source signals filtered with a 40 kHz high-pass filter in the coupon specimen.

	So mode at 522 kHz					Ao mode at 66 kHz				
Source	Distance, mm			Velocity, mm/μs		Distance, mm			Velocity, mm/μs	
depth, mm	60	120	180	Slope	Theoretical	60	120	180	Slope	Theoretical
2.037	33.8	60	99	1.82	1.78	-	-	-	-	-
0.783	-	-	-	-	-	33.8	61.9	91.2	2.09	2.62

large plate (those that lead to Figs. 1 and 2 and Table 1) are shown in Figs. 12 and 13 and Table 5 for the coupon. For the WT calculations the WS = 600 samples was used for both modes; and the FR and MF values used were 2 kHz and 400 kHz for the Ao mode and 3 kHz and 700 kHz for the So mode. The maximum WT magnitude arrival times were selected while ignoring reflections from the ends of the coupon specimen. Figure 12 shows the WTs for the coupon for the in-plane dipole at a depth of 2.037 mm. Figure 13 shows the coupon WTs for a depth of 0.783 mm. The source position for the results shown in Figs. 12 and 13, as well as Table 5, was located half-way across the coupon (12.7 mm form the side). Table 5 indicates the results were mixed. For the 2.037 mm depth and the So mode at 522 kHz, the slope-determined velocity of 1.82 mm/μs was the same as the large plate velocity of 1.82 mm/μs, but in the plot of distance versus arrival time the data did not fit the straight-line slope very well. For the 0.783 mm depth and the Ao mode at 66 kHz the slope-determined velocity in the coupon was 2.09 mm/μs (again data with a poor fit) which was 20 % lower than the value of 2.61 mm/μs in the large plate.

Table 6. Arrival times (μs) of the peak WT magnitude for in-plane dipole source at 2.35 mm depth and different distances from the coupon side. So mode at 522 kHz.

	Distance, mm			Velocity, mm/μs	
Case	60	120	180	Slope	Theoretical
Coupon, 3.31 mm	32.4	65.1	87.8	2.13	1.78
Coupon, 6.13 mm	36.4	77.7	103.8	1.75	1.78
Coupon, 12.7 mm	33.9	60	98.7	1.82	1.78
Large plate	31.9	64.6	97.9	1.82	1.78

To study the effect of side-to-side variation of the source position, we applied the same approach (522 kHz WT-peak arrival time) to the cases for the in-plane dipole at the mid-plane depth of 2.35 mm. Table 6 (same WT-parameters as for Table 5) shows the results (40 kHz high-pass data) for the coupon with the source at three different distances (12.7, 6.13, and 3.31 mm) from the coupon side compared to the equivalent large plate case. For convenience, the propagation distances are reported as 60, 120, 180 mm, but in determining the slope-based group velocities the actual straight-line distances from the source to the sensors were used. Table 6 clearly shows significant differences in the slope-determined group velocity (of the fundamental symmetric mode at a frequency of 522 kHz) as a function of transverse source position. Compared to the velocity determined from the large-plate signals (for the same case) the group velocity changes range from 0.6 % to 17 %. It is also clear from Table 6 that the arrival times at the different sensors vary over a considerable range compared to the large plate values, which were not influenced by the side-edge reflections. Figure 14 compares the differences in the WT magnitude versus time at 522 kHz for the large plate compared to the coupon specimen with the source at 3.31 mm from the coupon side. This figure is for the sensor located at the nominal propagation distance of 180 mm. The alteration of the peak arrival time in the coupon specimen is clearly visible along with the generally significantly larger magnitudes of the WT in that case.

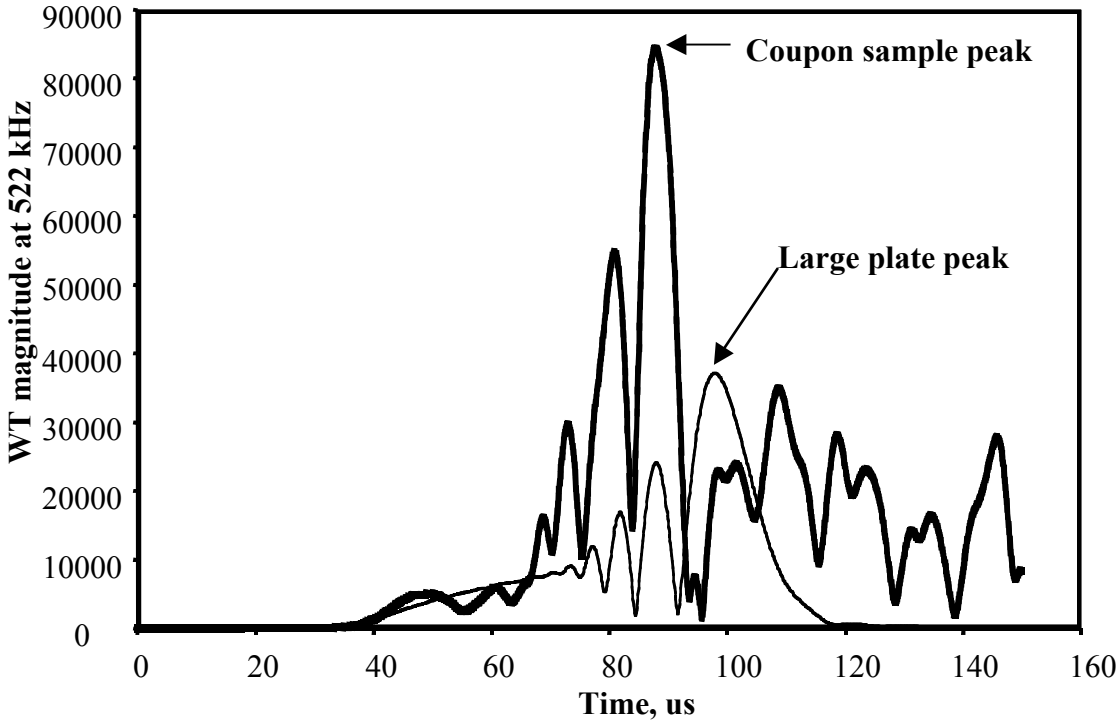

Fig. 14 WT magnitude at 522 kHz versus time for a large plate and coupon specimen. In both cases the source was an in-plane dipole at a depth of 2.35 mm and a propagation distance of 180 mm. The coupon source was located at 3.31 mm from the coupon side.

We conclude that significant and variable errors can be present in the arrival times for the coupon specimens when they are determined by the WT approach examined here. The errors in coupon-determined group velocities could be overcome by appropriate pencil lead-break data from a large-plate specimen of the same material and plate thickness as the coupon specimen, but arrival-time errors would remain. These errors would result in poor accuracy for source location calculations.

The effect of the side-to-side transverse source position was also examined using signals that had been filtered from 100 to 300 kHz. The WTs were calculated with high-resolution parameters (WS = 600 samples, MF = 400 kHz and FR = 2 kHz) for the in-plane dipole at a depth of 2.35 mm. Table 7 compares the three small coupon cases with the equivalent large-specimen results and the dispersion-curves-based group velocity at 262 kHz. As was the case above, the arrival time at maximum WT magnitude was selected by ignoring a magnitude maximum caused by reflections from the coupon-specimen's ends. The propagation distance versus the arrival times was plotted to determine the group velocity for each case of transverse source position. Compared to the large-plate data, the straight-line fits to the data for distance versus time were poor. The best fit was for the symmetrical center-line source position. But, even in that case, the group velocity was reduced by 13 % compared to the large-plate velocity. The group velocity determined when the source was located 6.13 mm from the coupon edge was very close to the result determined for the large plate. However, this was happenstance as the straight-line fit was very poor. Figure 15 shows the excellent fit and equation for the large plate as well as the significant error and typical scatter (relative to a straight line) of the three small-coupon cases. Thus, again, we conclude that side-edge reflections distort the determination of accurate arrival times. Obviously, inaccurate arrival times would lead to significant errors in source location.

Table 7. Arrival times (μs) of the peak WT magnitude for in-plane dipole sources at 2.35 mm depth and different distances from the coupon side. Signals were filtered from 100-300 kHz and the So mode at 262 kHz was used.

	Distance, mm			Velocity, mm/μs	
Case	60	120	180	Slope	Theoretical
Coupon, 3.31 mm	15.3	34.8	46.8	3.74	4.89
Coupon, 6.13 mm	26.4	44.5	47	4.89	4.89
Coupon, 12.7 mm	19.4	34.4	47.6	4.25	4.89
Large plate	15.8	28.3	40.5	4.86	4.89

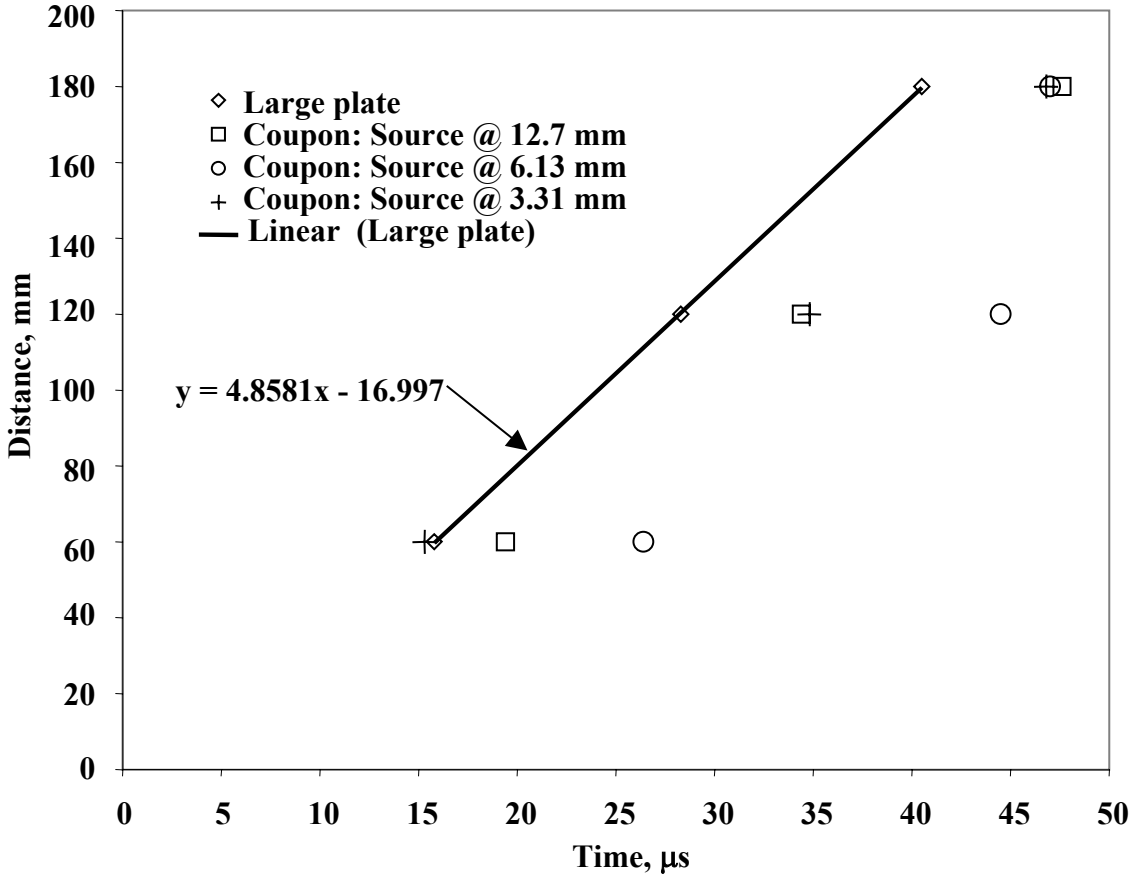

Fig. 15 Excellent fit of distance versus arrival time from WT peak magnitude at 262 kHz for large plate as compared to scatter and consequent lack of straight line fit for coupon specimen cases with variation in source distance from specimen side. AE signals were filtered from 100 to 300 kHz prior to the WT. Source was an in-plane dipole at a depth of 2.35 mm below the plate surface.

8. Conclusions

A. Source Location–Large Plates

- Excellent straight-line correlations of propagation distance versus the WT-based arrival times of the fundamental modes at fixed frequencies indicate that source location in large plates

can be significantly enhanced by use of WT results compared to that possible with fixed thresholds and an assumed constant group velocity.

- Since the amount of energy in a particular mode depends on the source depth, it will be necessary to first select the mode with the dominant energy in each AE signal. Then WT-based arrival times of the maximum WT magnitude of the experimental AE signals can be obtained from that mode at a selected frequency.
- In experimental situations, carefully applied pencil-lead breaks can be used to determine the key frequency to use for each dominant mode. Then only the WT-based arrival times and peak magnitudes at these frequencies need to be extracted. The source location can then be directly calculated from the arrival times for the mode with the dominant peak magnitude. The group velocity for the calculation could be taken from dispersion curves for the selected mode and frequency or from a WT-based group velocity obtained during pre-experiments with careful pencil lead breaks.
- The technique for extraction of WT-based arrival times corresponding to a single group velocity was found to be applicable for both wideband and narrow-band signals.
- In the wideband case, the extraction of single-velocity arrival times was found to be robust in the presence of electronic noise even for signal-to-noise ratios as low as 1:1.

B. Source Location–Small Coupon Specimens

- The inherent multiple side-edge reflections present in small-coupon specimens complicate the use of the WT for the purpose of obtaining accurate source locations.

Acknowledgement

This work was partially supported by NASA Langley.

References

H. Cho, S. Ogawa and M. Takemoto, "Non-contact Laser Ultrasonics for Detecting Subsurface Lateral Defects", NDT and E International, **29**-5, 1996, 301-306.
Hayashi et al., 1999

M. R. Gorman, "Plate Wave Acoustic Emission", Journal of the Acoustic Society of America, **90** (1), 1990, 358-364.

M. A. Hamstad, "On Determination of Arrival Times for Acoustic Emission Source Location in Composites", *Proceedings AECM-2*, Society of the Plastics Industry, New York, New York, 1986, pp. 202-208.

M. A. Hamstad, A. O'Gallagher and J. Gary, "Examination of the Application of a Wavelet Transform to Acoustic Emission Signals: Part 1. Source Identification", Journal of Acoustic Emission, **20**, 2002, 39-61. (preceding paper)

M. A. Hamstad and K. S. Downs, "On Characterization and Location of Acoustic Emission Sources in Real Size Composite Structures – A Waveform Study", Journal of Acoustic Emission, **13**, No. 1–2, 1995, 31-41.

Yasuhisa Hayashi, Shingo Ogawa, Hideo Cho and Mikio Takemoto, “Non-contact estimation of thickness and elastic properties of metallic foils by the wavelet transform of laser-generated Lamb waves”, NDT and E International, **32**-1, 1999, 21-27.

Hyunjo Jeong and Young-Su Jang, “Fracture Source Location in Thin Plates Using the Wavelet Transform of Dispersive Waves”, IEEE Transactions on Ultrasonics, Ferroelectrics and Frequency Control, **47**-3, 2000, 612-619.

O.Y. Kwon and Y.C. Joo, “Source Location in Plates by Using Wavelet Transform of AE Signals”, Journal of Acoustic Emission, **18**, 2000, S212-221.

M. Takemoto, H. Nishino and K. Ono, "Wavelet Transform - Applications to AE Signal Analysis", *Acoustic Emission - Beyond the Millennium*, Elsevier, 2000, pp. 35-56.

H. Yamada, Y. Mizutani, H. Nishino, M. Takemoto and K. Ono, "Lamb Wave Source Location of Impact on Anisotropic Plates", Journal of Acoustic Emission, **18**, 2000, 51-60.

Steven M. Ziola and Michael R. Gorman, “Acoustic Emission Source Location in Thin Plates Using Crosscorrelation”, *Proceedings AECM-4*, The American Society for Nondestructive Testing Inc., Columbus, OH, 1992, pp. 411-417.